

Multipolar origin of bound states in the continuum

Zarina Sadrieva,^{1,*} Kristina Frizyuk,^{1,†} Mihail Petrov,¹ Yuri Kivshar,^{1,2} and Andrey Bogdanov¹

¹*ITMO University, St. Petersburg 197101, Russia*

²*Nonlinear Physics Center, Australian National University, Canberra ACT 2601, Australia*

Metasurfaces based on resonant subwavelength photonic structures enable novel ways of wavefront control and light focusing, underpinning a new generation of flat-optics devices. Recently emerged all-dielectric metasurfaces exhibit high-quality resonances underpinned by the physics of bound states in the continuum that drives many interesting concepts in photonics. Here we suggest a novel approach to explain the physics of bound photonic states embedded into the radiation continuum. We study dielectric metasurfaces composed of planar periodic arrays of Mie-resonant nanoparticles ("meta-atoms") which support both symmetry protected and accidental bound states in the continuum, and employ the multipole decomposition approach to reveal the physical mechanism of the formation of such nonradiating states in terms of multipolar modes generated by isolated meta-atoms. Based on the symmetry of the vector spherical harmonics, we identify the conditions for the existence of bound states in the continuum originating from the symmetries of both the lattice and the unit cell. Using this formalism we predict that metasurfaces with strongly suppressed spatial dispersion can support the bound states in the continuum with the wavevectors forming a line in the reciprocal space. Our results provide a new way for designing high-quality resonant photonic systems based on the physics of bound states in the continuum.

I. INTRODUCTION

The quest for compact photonic systems with high quality factor (Q factor) modes led to the rapid development of optical bound states in the continuum (BICs). BICs are non-radiating states, characterized by the resonant frequencies embedded to the continuum spectrum of radiating modes of the surrounding space [1, 2]. The BICs first appeared as a mathematical curiosity in quantum mechanics [3]. The discovery of BICs in optics immediately attracted broad attention (see, e.g., Refs. [4–6]) due to high potential in applications in communications [7, 8], lasing [9–12], filtering [13], and sensing [14–16]. Recent achievements in the field of BIC are discussed in Refs. [17–26].

Decoupling of the resonant mode from the radiative spectrum, which is the basic idea behind the BIC, can be interpreted in several equivalent ways. Within the coupled-mode theory, it corresponds to nullifying the coupling coefficient between the resonant mode and all radiation channels of the surrounding space [27]. Alternatively, the appearance of BICs is explained as vanishing of Fourier coefficients corresponding to open diffraction channels due to the symmetry of the photonic structure. At the particular high-symmetry points of the reciprocal space, for example, at the Γ point, the continuous spectrum is divided into the modes of different symmetry classes with respect to the reflectional and rotational symmetry of the photonic system. The bound states of one symmetry class can be found embedded in the continuum of another symmetry class, and their coupling is forbidden as long as the symmetry is preserved. Such

kind of BIC is called *symmetry-protected*, and they also allow interpretation in terms of topological charges defined by the number of times the polarization vectors winds around the BICs presented as vortex centers in the polarization field [28]. In contrast to the symmetry-protected BIC, the so-called *accidental BICs* [1, 28–31] can be observed out of the Γ -point due to an accidental nulling of the Fourier (coupling) coefficients via fine tuning of parameters of the photonic system. Such a mechanism is also known as Friedrich-Wintgen scenario [32].

Despite the number of existing approaches to understand the nature of BICs, there is still a room for further development of the theory. During the previous few years the electromagnetic multipole theory [33] has been extensively developed as a natural tool of nanophotonics dealing with the lowest (fundamental) resonances of the system. The main advantage of the multipole decomposition method (MDM) is that it provides a representation of an arbitrary field distribution as a superposition of the fields created by a set of multipoles [34, 35]. Namely, the multipole expansion has been widely used to determine the polarization and directivity patterns of the scattered field of single particles and their clusters both plasmonic and dielectric [34, 36] for a variety of applications such as polarization control device [35], dielectric nanoantenna [37], light demultiplexing [38], and others. A number of novel optical phenomena have been explained within the MDM such as anapole effect [39, 40], optomechanical phenomena [41, 42], and Kerker effect [43, 44].

In this work, we extend the MDM approach for explaining both symmetry protected and accidental BICs. We provide a theory of BICs origin in terms of MDM for a general case of any periodic structure and develop an analytical method, which determines the contribution of the vector spherical harmonics to the far field (Section II). Working in the vector spherical harmonics (VSH) basis, we take the advantage of the internal symmetry and

* z.sadrieva@metalab.ifmo.ru

† k.frizyuk@metalab.ifmo.ru

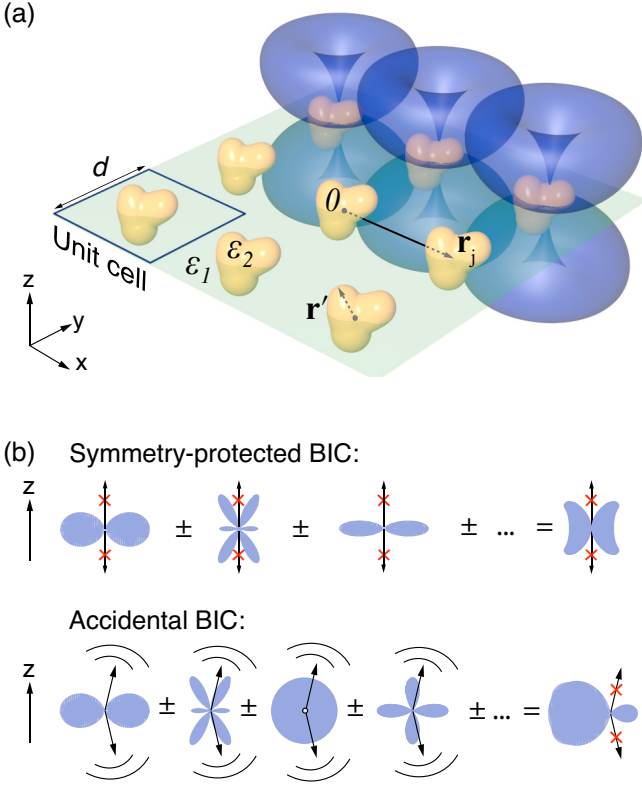


Figure 1. (a) Metasurface with square unit cell composed of dielectric meta-atoms. (b) The upper and lower panels show the formation mechanism of symmetry protected (at- Γ) and accidental (off- Γ) BIC.

provide the group-symmetry approach to identifying the BIC formation in terms of the unit cell and lattice symmetries (Section III). We implement field multipole expansion of the eigenmodes of a periodic two-dimensional (2D) photonic structure supporting BIC. We illustrate the developed technique by considering a 2D square array of spheres and extending it to the case of a photonic crystal slab with a 2D array of cylindrical holes (Section IV). The developed approach can be easily extended even further to periodic structures with other types of the unit cell and other lattice symmetries. The proposed method both provides a deeper understanding of the photonic BIC physics and gives a tool for an effective designing of high- Q resonant photonic systems.

II. MULTIPOLAR APPROACH

In this section we consider the modes of a two-dimensional periodic array of dielectric nanoparticles with arbitrary shape (see Fig. 1), and obtain an expression connecting the multipolar content of the field inside and outside the nanoparticles. We denote the VSHs as $\mathbf{M}_{p_r, m, n}(k, \mathbf{r})$ (magnetic) and $\mathbf{N}_{p_r, m, n}(k, \mathbf{r})$ (electric) relying on the definition presented in Ref. 45. We introduce an additional notation $\mathbf{W}_{p_i, p_r, m, n}$ for the both types of

VSHs, where inversion parity index $p_i = (-1)^{n+1}$ for $\mathbf{M}_{p_r, m, n}(k, \mathbf{r})$, and $p_i = (-1)^n$ for $\mathbf{N}_{p_r, m, n}(k, \mathbf{r})$. Index n is the multipole order, m varies from 0 to n , and $p_r = 1$ if $\mathbf{W}_{p_i, p_r, m, n}$ is even under reflection from $y = 0$ plane ($\varphi \rightarrow -\varphi$ in the spherical system), and $p_r = -1$ if it is odd [46].

In homogeneous medium with permittivity ε , any solution of the Helmholtz equation with wavevector $k = \sqrt{\varepsilon} \frac{\omega}{c}$ can be expanded in terms of electric and magnetic spherical harmonics [47]. The field inside the medium of j -th cell of the array \mathbf{E}^{in} can be written in terms of multipolar decomposition:

$$\mathbf{E}^{in}(\mathbf{r}) = \sum_{n=1}^{\infty} \sum_{\substack{m=0 \\ p_i, p_r}}^n E_0 [D_{p_i, p_r, m, n} \mathbf{W}_{p_i, p_r, m, n}^{(1)}(k_2, \mathbf{r}') e^{i(\mathbf{k}_b \cdot \mathbf{r}_j)}], \quad (1)$$

where $k_2 = \sqrt{\varepsilon_2} \frac{\omega}{c}$ is the wavevector in the material, the superscript (1) stands for spherical Bessel functions in the radial part of the VSH, \mathbf{k}_b is the Bloch vector, $\mathbf{r}' = \mathbf{r} - \mathbf{r}_j$, and \mathbf{r}_j is the position of a single sphere (see Fig. 1). $D_{p_i, p_r, m, n}$ are the coefficients of the multipolar decomposition, which will be discussed in Section III. In similar manner, the field outside the array is expressed as follows (see Appendix B):

$$\mathbf{E}(\mathbf{r}) = E_0 \sum_{\mathbf{K}, p_i, p_r, m, n} \tilde{D}_{p_i, p_r, m, n} \frac{V_b i^{-n}}{2\pi k_1} \times \iint_{-\infty}^{\infty} dk_{\parallel} \delta(\mathbf{k}_{\parallel} - \mathbf{k}_{\parallel} - \mathbf{K}) \frac{e^{i\mathbf{k}\mathbf{r}}}{k_z} \left[\mathbf{Y}_{p_i, p_r, m, n} \left(\frac{\mathbf{k}}{|\mathbf{k}|} \right) \right]. \quad (2)$$

Here \mathbf{K} is the reciprocal lattice vector, $k_z = \pm \sqrt{k_1^2 - k_{\parallel}^2}$, $|\mathbf{k}| = k_1 = \sqrt{\varepsilon_1} \frac{\omega}{c}$, V_b is the volume of the first Brillouin zone. The spherical vector functions $\mathbf{Y}(\mathbf{n})$ depend on the spherical coordinates of a unity vector \mathbf{n} and they are given in the Appendix A. Their symmetry coincides with the symmetry of \mathbf{W} -function with the identical indices. The relation between D and \tilde{D} is discussed in Appendix C, and for the case of an array of spherical particles, coefficients \tilde{D} can be derived analytically.

The summation in Eq. (2) over the reciprocal vectors corresponding to open diffraction channels, i.e. the terms with real k_z , provides the contribution into the far field. For the frequencies below the diffraction limit, only the zero-order term with $\mathbf{K} = 0$ gives non-zero contribution to the far field:

$$\mathbf{E}(\mathbf{r}) = \frac{E_0 V_b}{2\pi k_1 k_{1z}} e^{i\mathbf{k}_1 \mathbf{r}} \sum_{\substack{p_i, p_r, \\ m, n}} i^{-n} \tilde{D}_{p_i, p_r, m, n} \left[\mathbf{Y}_{p_i, p_r, m, n} \left(\frac{\mathbf{k}_1}{k_1} \right) \right], \quad (3)$$

where $\mathbf{k}_{1\parallel} = \mathbf{k}_b$, and $k_{1z} = \pm \sqrt{k_1^2 - k_b^2}$. According to Eq. (3), the contribution of the multipole with numbers p_i, p_r, m, n into the far field in the direction defined by the wave vector \mathbf{k}_1 is proportional to the multipole expansion coefficient \tilde{D} and the value of spherical vector

function \mathbf{Y} in the given direction. Equation (3) provides the correspondence between the radiation pattern of a single unit cell and the far-field properties of the whole infinite array allowing for interpreting the BIC in terms of MDM. In strong contrast to a single nanoparticle, where each multipole contributes to the far field, in case of a subdiffractive array there might be direction, where non of the multipole gives any contribution, or alternatively the non-zero contribution of different terms may eventually sum up to zero. The formulated alternative gives a sharp distinction between the symmetry protected and accidental BIC.

At- Γ -point BIC. The Γ -point BIC corresponds to the absence of the far-field radiation in the direction along the z -axis. Due to the structure of VSH, it appears that a number of multipoles do not radiate in the vertical direction along the z -axis. If the field inside a single unit cell consists only of such multipoles, there will be no total radiation in z -direction. This simple fact is illustrated in the upper panel in Fig. 1(b). Noticing that only $\mathbf{Y}_{p_i p_r, 1n}$ functions with $m=1$ are non-zero in parallel to the z -axis direction, we can conclude that at the Γ -point in the subdiffractive array all the modes which do not contain the harmonics with $m = 1$ are symmetry-protected BICs. This fundamental conclusion lies in the basis of recent experimental demonstration [9] of lasing with BIC in a 2D subdiffractive array of nanoparticles. The particular operational mode consisted of vertical dipoles oriented along the z -axis, thus, not contributing into the only open channel. There exist an approach [1, 28] that the eigenmodes at the Γ -point can radiate in the normal direction z if their fields are odd under C_2^z rotations, and do not have any other rotational symmetry of C_n^z -type. In terms of multipole moments, this follows from the fact that at the Γ -point any radiative mode should contain multipoles with $m = 1$. On the other hand, in virtue of the symmetry, the even modes have zero radiation losses, i.e. infinite radiation quality factor, which are known as symmetry-protected BICs.

Off- Γ BIC. Let us now turn to the case of accidental BIC description. In general case, coefficients D are complex numbers. They define the amplitudes and phase delay between the multipoles. However, in accordance with [29], if the structure has time reversal and inversion symmetry, the eigenmodes must satisfy the condition $\mathbf{E}(\mathbf{r}) = \mathbf{E}^*(-\mathbf{r})$. This fact imposes strict conditions on the multipoles' phases, because some of them are even under inversion and some of them are odd, the coefficient D_{-1p_r, m_n} before the odd ones must be imaginary. It follows that every term of the sum in Eq. (3) is purely real, and all multipoles are in-phase or anti-phase. All coefficients depend on \mathbf{k} -vector and structure's parameters and in a case of the off- Γ BICs this sum turns to zero. In other words, for the particular \mathbf{k}_1 all vector harmonics add up to zero in the direction of \mathbf{k}_1 , analogously to the anti-Kerker effect, because they are already in phase and only amplitudes are modulated while \mathbf{k} -vector is changed [Fig. 1(b), lower panel]. One can intuitively understand acci-

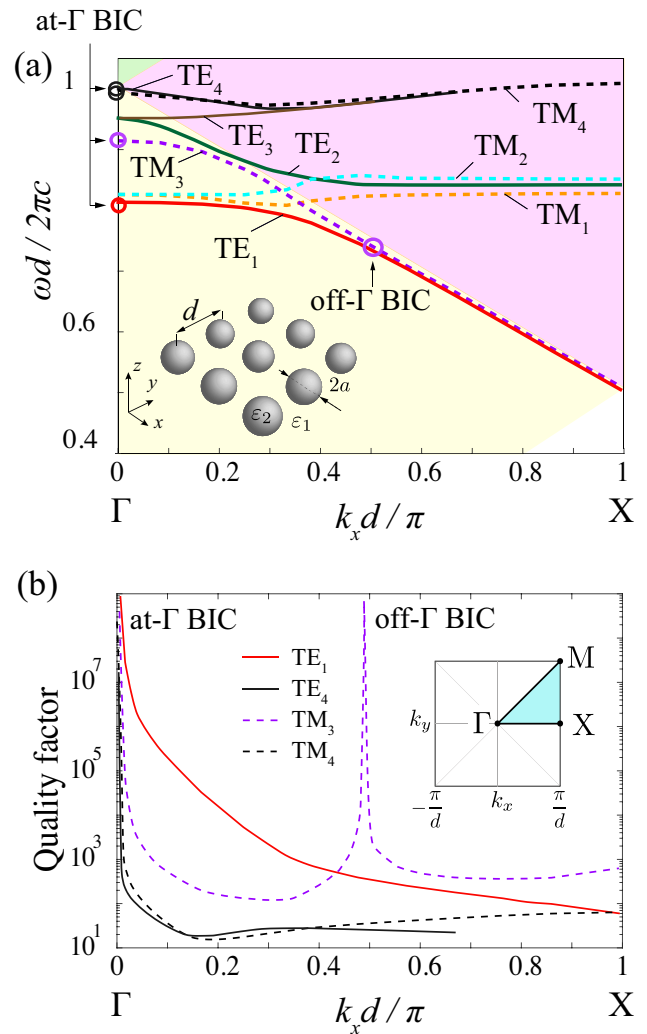
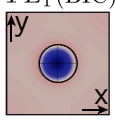
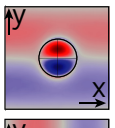
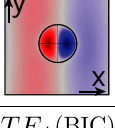
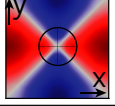


Figure 2. (a) Band diagram for the square periodic array of dielectric spheres at the $\overline{\Gamma X}$ -valley. Period $d = 600$ nm, nanosphere radius $a=100$ nm, dielectric permittivity of the spheres is $\epsilon_2=12$, medium permittivity is $\epsilon_1=1$. Modes TE_1 , TE_4 , TM_3 , TM_4 , are symmetry-protected BICs at the Γ -point. (b) Q-factor of the TM_3 mode in the $\overline{\Gamma X}$ -valley. At the particular wave vector, Q-factor tends to infinity and the accidental BIC appears.

dental BIC (TM-polarized) via a toy dipole model composed of vertical electric and horizontal magnetic dipoles interfering destructively at some \mathbf{k} -vector [48].

The expansion coefficients $D_{p_i p_r, m_n}$ depend on shape of the nanoparticles, material parameters and symmetry of the lattice. Obviously, that the lattice symmetry should impose restrictions on $D_{p_i p_r, m_n}$ and some coefficients should vanish due to the symmetry. To explore these selection rules, we employ theoretical-group approach.

Table I. Multipolar content and irreducible representations of TE-modes at the Γ -point and at $\overline{\Gamma X}$ and $\overline{\Gamma M}$ valleys. Spherical harmonics for B_2 and A_1 representations at $\overline{\Gamma X}$ are provided at the right column of the table. The multipoles for the same representations at $\overline{\Gamma M}$ can be obtained by rotation by $\pi/4$. Imaginary unit means that coefficients D before these harmonics must be imaginary. The z -component of the magnetic field H_z is shown in the inserts.

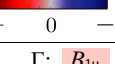
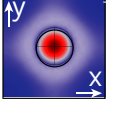
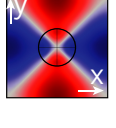
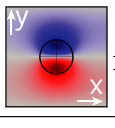
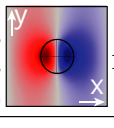
 Γ : H_z -field profile, representation, spherical harmonics	$\overline{\Gamma X}, \overline{\Gamma M}$	spherical harmonics for B_2 ($\overline{\Gamma X}$):
TE_1 (BIC)  Γ : A_{2g} $M_{-101}, M_{-103}, N_{-144}, M_{-105}, M_{-145}$	$\overline{\Gamma X}$: B_2 $\overline{\Gamma M}$: B_2	$iN_{-111}, N_{-122}, iN_{-113}, iN_{-133}, N_{-124}, N_{-144}, M_{-101}, iM_{-112}, M_{-103}, M_{-123},$
TE_2, TE_3   Γ : E_u $N_{111}, M_{112}, N_{113}, N_{133}, M_{114}, M_{134}$ $N_{-111}, M_{-112}, N_{-113}, N_{-133}, M_{-114}, M_{-134}$	$\overline{\Gamma X}$: $B_2 + A_1$ $\overline{\Gamma M}$: $B_2 + A_1$	spherical harmonics for A_1 ($\overline{\Gamma X}$): $iN_{111}, N_{102}, N_{122}, iN_{113}, iN_{133}, N_{104}, N_{124}, N_{144}, iM_{112}, M_{123}, iM_{114}, iM_{134}$
TE_4 (BIC)  Γ : B_{2g} $N_{-122}, M_{-123}, N_{-124}, M_{-125}, N_{-126}, N_{-166}$	$\overline{\Gamma X}$: B_2 $\overline{\Gamma M}$: A_1	

III. SYMMETRY APPROACH

The group-theoretic approach is a powerful method which is widely used for analyzing the properties of periodic photonic system [30, 49–52]. In this section, we apply this method to reveal which of the coefficients D_{p_i, p_r, m_n} are non-zero in accordance with the mode symmetry imposed by the symmetry of the periodic structure [53, 54] and to explain the formation of BIC. To make further analysis more illustrative we will provide it by the example of a square periodic array of dielectric spheres shown in the inset in Fig. 2(a). Nevertheless, it is necessary to highlight that further considerations remain true for any kind of structures with square lattice with the point group symmetry D_{4h} .

Figure 2(a) shows the dispersion of eigenmodes along the $\overline{\Gamma X}$ direction for a square periodic array of dielectric spheres with permittivity $\epsilon_2 = 12$ embedded in the air with permittivity $\epsilon_1 = 1$. The dispersion is calculated numerically using COMSOL Multiphysics package. The radius of the spheres is $a = 100$ nm and the period of the array is $d = 600$ nm. By the analogy with a dielectric slab waveguide, the eigenmodes of the 2D array are split into transverse electric (TE) and transverse magnetic modes (TM), which have mainly the z -component of magnetic and electric field, correspondingly. Figure 2(b) shows the

Table II. Multipolar content and irreducible representations of TM-modes. The z -component of the electric field E_z is shown in the inserts. Note that representations can be obtained by replacing for TE-modes $A_2 \leftrightarrow A_1, B_2 \leftrightarrow B_1, u \leftrightarrow g$, and multipolar content can be obtained by replacing $p_r \leftrightarrow -p_r, M \leftrightarrow N$

Γ -point: E_z -field profile, representations, spherical harmonics, representations in $\overline{\Gamma X}$ and $\overline{\Gamma M}$				
	Γ :			
TM_3 (BIC) 	Γ : A_{1u}	TM_4 (BIC) 	Γ : B_{1u}	
	$N_{101}, N_{103}, M_{144}, N_{105}, N_{145}, M_{146}$		$M_{122}, N_{123}, M_{124}, N_{125}, M_{126}, M_{166}$	
$\overline{\Gamma X}$: B_1	$\overline{\Gamma M}$: B_1	$\overline{\Gamma X}$: B_1	$\overline{\Gamma M}$: A_2	
TM_1 	$M_{-111}, N_{-112}, M_{-113}, M_{-133}, N_{-114}, N_{-134}$	TM_2 	$M_{111}, N_{112}, M_{113}, M_{133}, N_{114}, N_{134}$	Γ : E_g
				$\overline{\Gamma X}$: $B_1 + A_2$
				$\overline{\Gamma M}$: $B_1 + A_2$

dependence of the Q-factor on the Bloch wavenumber k_x for the modes, which are BICs at the Γ -point. One can see that additionally to at- Γ -BIC, TM_3 mode turns into off-BIC in the middle of the Brillouin band (accidental BIC).

The eigenmodes of periodic structures have certain symmetry in accordance with the fact that every mode is transformed by an irreducible representation of the structure's symmetry group [55, 56]. While Bloch functions are already the basis functions of the translation group irreducible representation labeled by \mathbf{k}_b , under point group operations the basis functions with different \mathbf{k}_b transform through each other. They carry high-dimensional representations of the space group. We are interested in the multipolar content of the mode with particular \mathbf{k}_b , so we look at the point group of \mathbf{k}_b , i.e. the subgroup of the whole point group, which transforms the \mathbf{k}_b into an equivalent. Note that symmetry of the unit cell should be also taken into account since it alters the point group of the full structure.

At the Γ -point, the group of \mathbf{k}_b is the whole group D_{4h} , $\mathbf{k}_b = 0$ and it is not transformed. At $\overline{\Gamma X}$ -valleys the point group of \mathbf{k}_b is C_{2v} , which consists of π -rotation around the x - or y - axis and two plane reflections at $z = 0$ and at $y = 0$ or $x = 0$. These operations keep vector \mathbf{k}_b invariant. Analogously, in the $\overline{\Gamma M}$ -valley the group is also C_{2v} . Solutions with particular \mathbf{k}_b are transformed by one of the \mathbf{k}_b -group irreducible representations. Thus, since the solution is transformed as a basis function of some particular representation, the multipolar content is strictly limited. Namely, all the multipoles with non-zero contribution must be transformed by the similar irreducible representation of the \mathbf{k}_b -group. We will use common notations for irreducible representations, listed,

for example, in Ref. 57.

Γ -point. For example, we consider the TE_1 mode of the square array, which is transformed by A_{2g} at the Γ -point. Under the transformations of D_{4h} group the only low-order multipoles transformed by A_{2g} are magnetic dipole \mathbf{M}_{-101} , magnetic octupole \mathbf{M}_{-103} , and electric hexadecapole \mathbf{N}_{-144} . All of them are invariant under C_4 rotations, even under inversion and $z = 0$ -plane reflection and odd under other D_{4h} transformations. Higher-order multipoles which behave in the same way are also presented in the multipolar content of this mode.

Analogously, we classify all possible multipoles at the Γ -point in accordance with their symmetry and provide the tables with multipolar content of the modes (Tables I and II). Note, that TE_2 and TE_3 modes degenerate, and they transform through each other as two basis functions of the representation E_u .

$\overline{\Gamma X}$ valley. After the symmetry reduction, when we step out the Γ -point into $\overline{\Gamma X}$ valley, some symmetry operations remain, e.g. mirror reflections in $z = 0$ and $y = 0$ planes and rotation by π around the x -axis. Eigenmodes must behave in the same way under these symmetry operations, as at the Γ -point.

As an example, we consider TE_1 mode, which transforms by A_{2g} at the Γ -point, and TM_3 mode (A_{1u}) at the $\overline{\Gamma X}$ valley. Using the compatibility relations [52], we obtain that the mode which transforms by A_{2g} at the Γ -point is transformed under B_2 representation of the group C_{2v} in the $\overline{\Gamma X}$ valley. The TM_3 -mode, which is A_{1u} at the Γ , is transformed under B_1 in $\overline{\Gamma X}$. For the A_{2g} mode at the Γ -point, which is odd under reflection in the $y = 0$ plane and π -rotation around x and even under reflection in $z = 0$ plane, the only possible multipoles in $\overline{\Gamma X}$ valley should have the same symmetry properties. For the A_{1u} mode the possible multipoles in the $\overline{\Gamma X}$ valley must be odd under reflection in the $z = 0$ plane and π -rotation and even under reflection in the $x = 0$ plane. Low-order possible multipoles in the $\overline{\Gamma X}$ valley are listed at the right column of Table I for TE modes, and for TM modes are easily derived by replacing $A_2 \leftrightarrow A_1, B_2 \leftrightarrow B_1, u \leftrightarrow g, p_r \leftrightarrow -p_r, \mathbf{M} \leftrightarrow \mathbf{N}$. Analogously, for the $\overline{\Gamma M}$ valley we have specific symmetry in the $x = y$ or $x = -y$ direction and possible multipoles are the same as those which are transformed by the same representation in $\overline{\Gamma X}$ valley, but rotated by $\pi/4$ with help of Wigner D-matrixes [58, 59].

IV. MULTIPOLAR COMPOSITION OF THE EIGENMODES IN PERIODIC STRUCTURES

A. Multipole analysis of metasurfaces and photonic crystal slabs

Before applying the developed approach to certain structures, we would like to emphasize that the power of the group-theoretic approach and multipole decomposition method is that these methods applied equally for

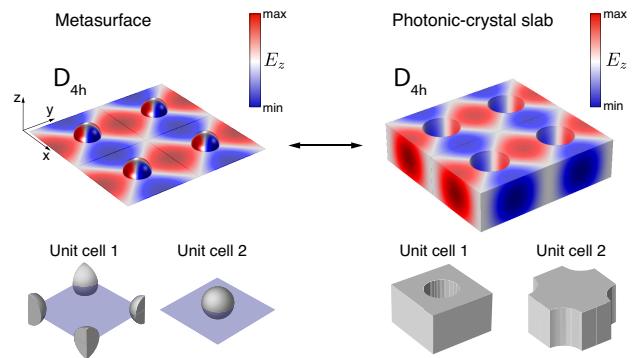


Figure 3. Distribution of E_z component of electric field of the modes corresponding to the same irreducible representation B_{1u} (see Table II) in the photonic-crystal slab and metasurface.

metasurfaces (arrays of meta-atoms) and photonics crystal slabs (slabs with holes). For example, a square array of dielectric spheres and dielectric slab with circular holes arranged in a square lattice are identical from the point of view of the group theory. Therefore, these structures have the same classification of eigenmodes and, that more important, the same multipole content (Mie-resonances). The difference will be only in amplitudes of the multipole coefficients.

At first glance it may seem unphysical to characterize the unit cell with a hole by Mie resonances. This contradiction can be eliminated by means of the proper choice of the unit cell. Indeed, Fig. 3 shows the modes of the photonic-crystal slab and metasurface corresponding to the same irreducible representation B_{1u} (see Table II). One can see that the mode structures are completely identical. However it is more physical to assign Mie resonances not the unit cell with a hole but to the cross-like shape unit cell (see the low panel in Fig. 3). In particular, it was shown in [60] that the optical response of both photonic-crystal slab and metasurface is dominated by the electric and magnetic Mie-type dipole resonances, and both type of the structures provides 2π phase control of light.

B. Periodic arrays of dielectric spheres

In order to understand how the interference of the multipole moments forms the BICs, we applied a method of multipole decomposition by expanding the eigenmodes fields inside the nanoparticles in terms of spherical harmonics [33, 34]. Figure 4 shows the numerical results for the multipole decomposition for TE_1 , TE_4 , and TM_4 modes at the Γ -point and in a point of the $\overline{\Gamma X}$ -valley. At the high-symmetry Γ -point only a small fraction of all possible multipoles is presented, while after lowering the symmetry extra multipoles appear out of the Γ -point. Figure 5 shows the numerical results for the multipole decomposition for TM_3 modes at the Γ -point, in a point

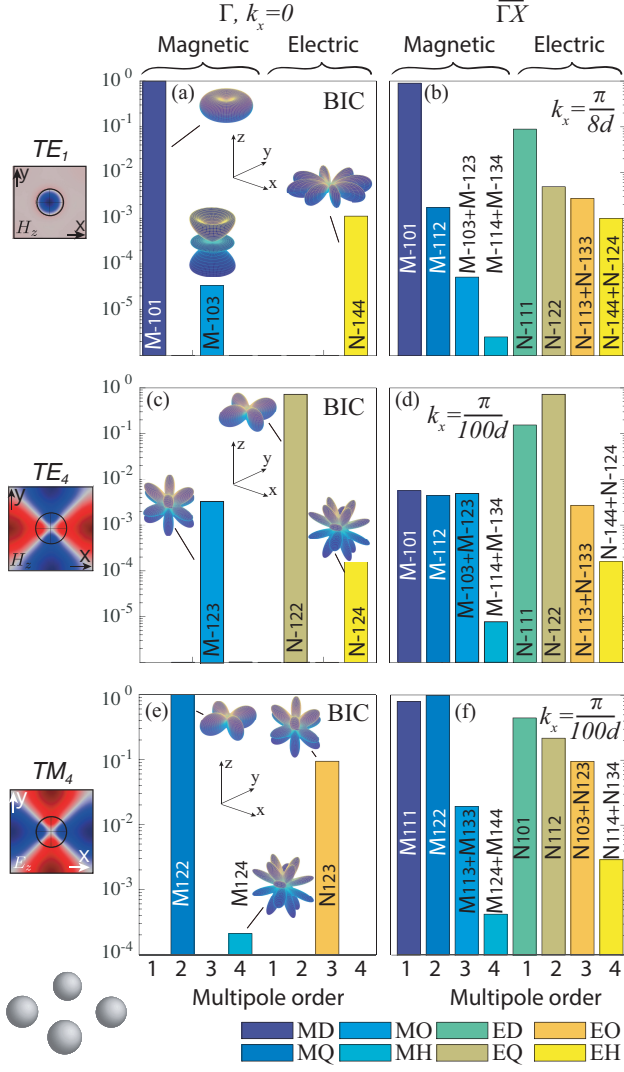


Figure 4. Multipolar content of TE_1 (a,b), TE_4 (c,d) and TM_4 (e,f) modes of the metasurface. Vertical axis shows values of normalized coefficients \tilde{D} . Horizontal axis shows multipolar order n . The letters in legend encodes the multipoles as follows: ED (MD) - electric (magnetic) dipole ($n = 1$), EQ (MQ) - electric (magnetic) quadrupole ($n = 2$), EO (MO) - electric (magnetic) octupole ($n = 3$), EH (MH) - electric (magnetic) hexadecapole ($n = 4$).

of the ΓX -valley, and at the off- Γ BIC.

At- Γ -BIC. One can see, that for at- Γ TE_1 (A_{2g}) BIC-mode magnetic dipole along the z -axis (\mathbf{M}_{-101}) is mainly contributed [Fig. 4(a)]. Its directivity pattern restricts radiation along the z -axis, and the radiation patterns of all remaining multipoles at the Γ -point are also zero along the z -axis. Other directions of radiation are forbidden due to the subdiffraction regime. Similarly, at- Γ TM_3 (A_{1u}) BIC is formed by electric dipole along the z -axis (\mathbf{N}_{101}) mostly, prohibiting the radiation in vertical direction itself [Fig. 5(a)]. The TE_4 (B_{2g}) and TM_4 (B_{1u}) modes' lowest multipoles are the electric

quadrupole \mathbf{N}_{-122} and the magnetic quadrupole \mathbf{M}_{122} respectively. They have $m = 2$, which also prohibits the radiation [Figs. 4(c) and 4(e)]. In contrast to BICs, the radiative modes (E_g, E_u) degenerate at the Γ point since they are transformed by the two-dimensional representations. From the symmetry-group approach, we know that $TE_{2,3}$ and $TM_{1,2}$ modes contain electric $\mathbf{N}_{\pm 111}$ and magnetic $\mathbf{M}_{\pm 111}$ spherical harmonics. The numerical multipole expansion shows that degenerated modes contain in-plane electric or magnetic dipole moments as the main contribution. These numerical results validate the symmetry-group approach for the system with square lattice, confirming that any symmetry-protected BIC is characterized by multipole moments with $m \neq 1$.

Off- Γ BIC. Away from the Γ -point other multipoles appear in decomposition [Figs. 4(b), 4(d), 4(f) and 5(b)] and BIC is destroyed turning into a resonance state. As mentioned earlier in the Section II, the accidental off- Γ BICs is formed due to either in- or anti-phase contributions of different multipoles. We obtain the same result for TM_3 mode with off- Γ BIC in the ΓX -valley [Fig. 5(c)]. This mode is transformed by B_1 representation and consist of the multipoles, which are odd under reflection in the $z = 0$ plane and π -rotation around x -axis and even under $y = 0$ reflection, eg. $i\mathbf{N}_{101}, \mathbf{N}_{112}, i\mathbf{N}_{103}, i\mathbf{N}_{123}, \mathbf{M}_{111}, i\mathbf{M}_{122}, \mathbf{M}_{113}, \mathbf{M}_{133}$. They sum up into TM -polarized wave in the direction given by vector \mathbf{k}_1 and cancel each other in the off- Γ point forming accidental BIC, shown in Fig. 2(b). In addition to all, it is well known, that the $z = 0$ plane reflection symmetry of the structure is required to obtain the off- Γ BIC [29]. Indeed, in lack of such symmetry, each mode would contain both odd and even multipoles under reflection in the $z = 0$ plane. To restrict the radiation both in the upper- and lower half-spaces, odd and even multipoles should be summed up into zero independently, while for the symmetric structure only one type of multipoles is presented for each mode, which makes it possible to achieve the BIC by tuning the structure parameters.

C. Photonic crystal slab

We extend our approach beyond the 2D array of spheres and apply it to the photonic crystal slab of the same symmetry. We consider a dielectric slab with a square array of cylindrical holes studied in [29]. Both at- Γ (symmetry-protected) and off- Γ (accidental) BICs appear in the lowest TM band referred to as TM_h . This mode has the field profile of the same symmetry as the TM_4 mode of the array of the spheres and is transformed by B_{1u} representation.

The description of the far field defined by the Eq. (3) is still valid, but the coefficients $\tilde{D}_{p_i p_r m n}$ in general cannot be expressed analytically through $D_{p_i p_r m n}$ (see Appendix C). However, only the multipoles which are presented in the field inside the slab contribute into far field,

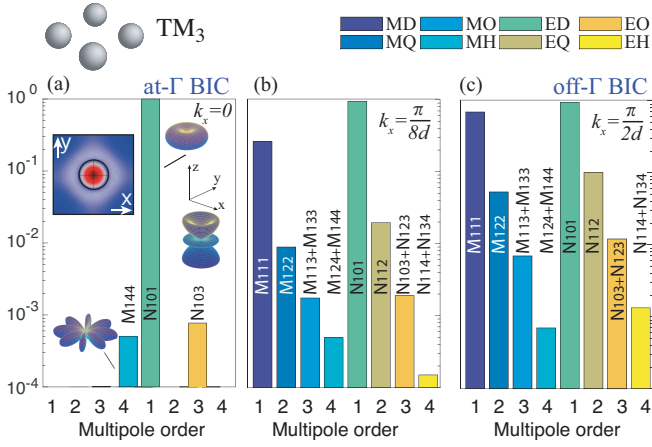


Figure 5. Multipolar content of TM_3 mode of the metasurface for three k_x Bloch vectors corresponding to the symmetry-protected BIC(a), leaky mode (b) and accidental BIC (c). Vertical axis shows values of normalized \tilde{D} coefficients, horizontal axis shows multipolar order n . The letters in legend encodes the multipoles as follows: ED (MD) - electric (magnetic) dipole ($n = 1$), EQ (MQ) - electric (magnetic) quadrupole ($n = 2$), EO (MO) - electric (magnetic) octupole ($n = 3$), EH (MH) - electric (magnetic) hexadecapole ($n = 4$).

$\tilde{D}_{p_i p_r m n} = 0$ if $D_{p_i p_r m n} = 0$. The multipolar content for the considered slab is the same as in the periodic array of spheres because the modes of the slab have the same symmetry as the modes of the array. The multipole decomposition of TM_h mode [Fig. 6(a)] reveals that a magnetic quadrupole \mathbf{M}_{122} and electric octupole \mathbf{N}_{123} make the major contribution to the at- Γ BIC, as well as to the TM_4 mode of the array of the spheres. However, the B_{1u} mode of the photonic crystal slab is the lowest-energy TM mode while for the array of spheres it has the highest energy among modes under diffraction limit. Due to the variational principle [61], for the mode of such symmetry, the electric field is more concentrated inside the high-index material in case of photonic crystal slab, minimizing the energy of the mode. Although dispersion curves $\omega(k)$ of the modes TM_4 and TM_h behave completely differently, multipole decomposition proves a common origin of them. At the Γ -point, we obtain contributions of multipoles only with $m = 2, 6, 10$, etc. for both modes, and none of these multipoles contribute in the far-field. At the $\overline{\Gamma X}$ -valley, the multipolar content of the TM_4 and TM_h is similar [Figs. 4(e), 4(f), 6(a), and 6(b)]. However, for the TM_h it is possible to obtain an accidental off- Γ BIC in the $\overline{\Gamma X}$ -valley [Fig. 6(c)]. Away from the Γ -point, multipole contributions change smoothly keeping the multipolar content invariable, and at a particular wave vector k_x multipoles interfere destructively forming the accidental BIC.

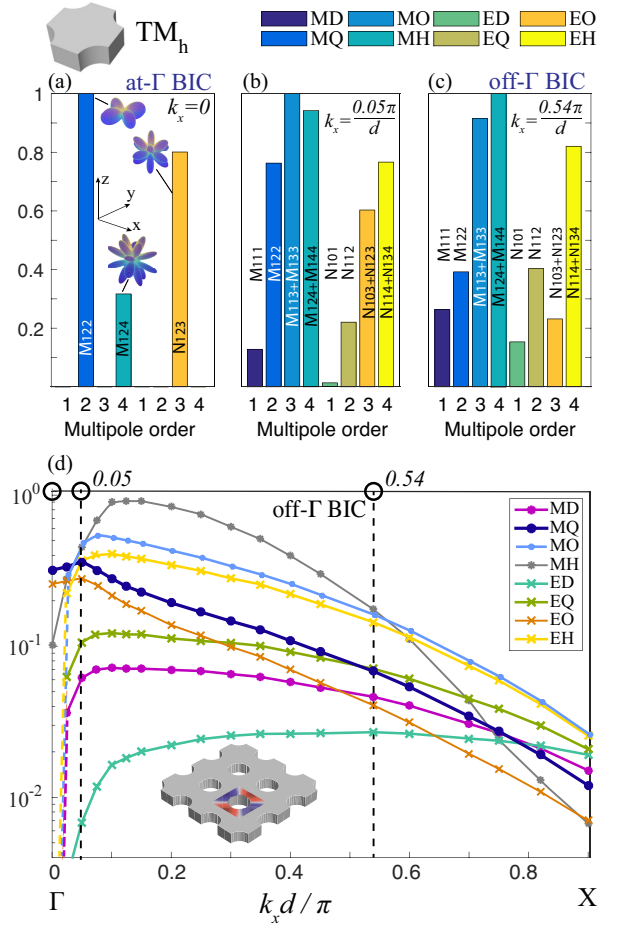


Figure 6. Multipolar content of TM_h mode of the PhC slab for three k_x Bloch vectors corresponding to the symmetry-protected BIC(a), leaky mode (b) and accidental BIC (c). Vertical axis shows values of normalized \tilde{D} coefficients, horizontal axis shows multipolar order n . Figure (d) depicts how the multipolar contributions change along $\overline{\Gamma X}$ valley. The letters in legend encodes the multipoles as follows: ED (MD) - electric (magnetic) dipole ($n = 1$), EQ (MQ) - electric (magnetic) quadrupole ($n = 2$), EO (MO) - electric (magnetic) octupole ($n = 3$), EH (MH) - electric (magnetic) hexadecapole ($n = 4$).

V. SUMMARY AND OUTLOOK

Importantly, our approach based on the multipole decomposition analysis of individual meta-atoms not only explains clearly and in simple physical terms the origin of both symmetry protected and accidental bound states in the continuum, but it has also a prediction power and may be employed for both prediction and engineering different types of BICs. As an example, we consider a metasurface consisting of meta-atoms packed in a sub-wavelength 2D lattice, which are polarized purely as octupoles, for example, \mathbf{M}_{-103} (see Fig. 7). Each octupole of this type has a nodal cone and, therefore, we can expect that in a periodic subwavelength array of such meta-

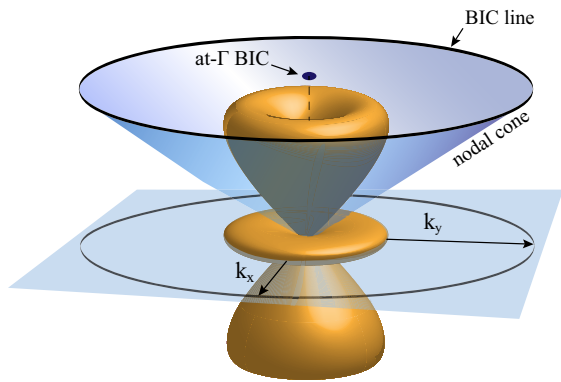


Figure 7. BIC line formed by metasurface composed of point octupoles with radiation pattern \mathbf{N}_{103} .

atoms, BICs form a line in the reciprocal space. However, to observe this phenomenon, the effective polarizability of the unit cell accounting for the interaction between all meta-atoms should not depend on the Bloch wavenumber or have very weak dependence. In other words, the line of BIC could be observed in metasurfaces with suppressed spatial dispersion that is still a challenging problem. Interestingly, such a kind of BIC will be observed for the same directions independently on the lattice symmetry of the metasurface.

We can expand this discussion even further, by adding \mathbf{M}_{-101} dipole mode into consideration. To obtain the Q-factor of the at- Γ BIC, we should find the dependence of energy loss rate on \mathbf{k} -vector in Eq. (3), assuming stored energy is almost constant when $\theta_k \rightarrow 0$. The asymptotic behavior for $\theta_k \rightarrow 0$ of $\mathbf{Y}_{p_i p_r m n} \left(\frac{\mathbf{k}}{|\mathbf{k}|} \right)$ functions is defined by $\frac{dP_n^m(\cos \theta_k)}{d\theta_k}$. So, $Y_{1-103} \left(\frac{\mathbf{k}}{|\mathbf{k}|} \right) \propto (-6k_x + 17k_x^3/2)\mathbf{e}_\varphi$, and $Y_{1-101} \left(\frac{\mathbf{k}}{|\mathbf{k}|} \right) \propto (k_x - k_x^3/6)\mathbf{e}_\varphi$. We can manage their relative contribution, and at particular point when coefficient before dipole is six times larger, we obtain that linear terms cancel each other and field asymptotic is proportional to k_x^3 , so the quality-factor growth is proportional to k_x^{-6} . Similar effect was observed in [21] for

the photonic crystal slab. However, considering realistic situations, we should take into account all possible multipolar contributions, including terms with $m = 1$, where the multipole contribution growth rate plays role but not the asymptotic behavior. Thus, the multipole origin of BIC makes a new query for metasurfaces with a suppressed spatial dispersion.

In summary, we have demonstrated that symmetry-protected bound states in the continuum in dielectric metasurfaces and photonic crystal slabs at the frequencies below the diffraction limit are associated with the multipole moments of the elementary meta-atoms which do not radiate in the transverse direction. For any type of metasurfaces, the symmetry-protected bound states in the continuum can be observed only if there exist no multipoles with the azimuthal index $m = 1$ in the multipole decomposition. The symmetry approach allows to determine which multipolar content the lattice eigenmodes have, and it can be analogously applied to the structures with different symmetries, for example, hexagonal lattices or arrays of nanoparticles of an arbitrary shape and in-plane broken symmetry. Similarly, we have revealed that the accidental bound state in the continuum corresponding to an off- Γ point in the reciprocal space is formed due to destructive interference of the multipole fields in the far-zone. We have provided the general tools for the analysis of bound states in the continuum based on the irreducible representation of the appropriate photonic band. We believe that our results will provide a new way for designing high-quality resonant photonic systems based on the physics of bound states in the continuum.

ACKNOWLEDGMENTS

The authors acknowledge useful discussions with I.D. Avdeev. Y.K. acknowledges a support from the Strategic Fund of the Australian National University. Z. S. acknowledges support from the Foundation for the Advancement of Theoretical Physics and Mathematics "BASIS" (Russia).

Z.S. and K.F. contributed equally to this work.

-
- [1] C. W. Hsu, Bo Zhen, A. D. Stone, J. D. Joannopoulos, and M. Soljačić, "Bound states in the continuum," *Nat. Rev. Mater.* **1**, 16048 (2016).
 - [2] K. Koshelev, A. Bogdanov, and Yu. Kivshar, "Metaoptics and bound states in the continuum," *Sci. Bull.* (2018).
 - [3] J. Von Neumann and E. P. Wigner, "Über merkwürdige diskrete Eigenwerte," *Phys. Z.* , 465–467 (1929).
 - [4] P. Paddon and Jeff F. Young, "Two-dimensional vector-coupled-mode theory for textured planar waveguides," *Phys. Rev. B* **61**, 2090–2101 (2000).
 - [5] E. N. Bulgakov and A. F. Sadreev, "Bound states in the continuum in photonic waveguides inspired by defects," *Phys. Rev. B* **78**, 075105 (2008).
 - [6] D. C. Marinica, A. G. Borisov, and S. V. Shabanov, "Bound States in the Continuum in Photonics," *Phys. Rev. Lett.* **100**, 183902 (2008).
 - [7] F. Dreisow, A. Szameit, M. Heinrich, R. Keil, S. Nolte, A. Tünnermann, and S. Longhi, "Adiabatic transfer of light via a continuum in optical waveguides." *Opt. Lett.* **34**, 2405–2407 (2009).
 - [8] C. M. Gentry and M. A. Popović, "Dark state lasers," *Opt. Lett.* **39**, 4136 (2014).
 - [9] S. T. Ha, Y. H. Fu, N. K. Emani, Z. Pan, R. M. Bakker, R. Paniagua-Dominguez, and A. I. Kuznetsov, "Directional lasing in resonant semiconductor nanoantenna ar-

- rays,” *Nat. Nanotechnol.* **13**, 1042–1047 (2018).
- [10] A. Kodigala, T. Lepetit, Q. Gu, B. Bahari, Y. Fainman, and B. Kanté, “Lasing action from photonic bound states in continuum,” *Nature* **541**, 196 (2017).
- [11] E. Penzo, S. Romano, Yu Wang, S. Dhuey, L. Dal Negro, V. Mocella, and S. Cabrini, “Patterning of electrically tunable light-emitting photonic structures demonstrating bound states in the continuum,” *J. Vac. Sci. Technol. B* **35**, 06G401 (2017).
- [12] M. Rybin and Yu. Kivshar, “Optical physics: Supercavity lasing,” *Nature* **541**, 164 (2017).
- [13] J. M. Foley and J. D. Phillips, “Normal incidence narrow-band transmission filtering capabilities using symmetry-protected modes of a subwavelength, dielectric grating,” *Opt. Lett.* **40**, 2637–2640 (2015).
- [14] J. M. Foley, S. M. Young, and J. D. Phillips, “Symmetry-protected mode coupling near normal incidence for narrow-band transmission filtering in a dielectric grating,” *Phys. Rev. B* **89**, 165111 (2014).
- [15] S. Romano, A. Lamberti, M. Masullo, E. Penzo, S. Cabrini, I. Rendina, and V. Mocella, “Optical biosensors based on photonic crystals supporting bound states in the continuum,” *Materials* **11**, 526 (2018).
- [16] S. Romano, G. Zito, S. Torino, G. Calafiore, E. Penzo, G. Coppola, S. Cabrini, I. Rendina, and V. Mocella, “Label-free sensing of ultralow-weight molecules with all-dielectric metasurfaces supporting bound states in the continuum,” *Photon. Res.* **6**, 726–733 (2018).
- [17] L. Carletti, K. Koshelev, C. De Angelis, and Yu. Kivshar, “Giant nonlinear response at the nanoscale driven by bound states in the continuum,” *Phys. Rev. Lett.* **121**, 033903 (2018).
- [18] X. Gao, C. W. Hsu, B. Zhen, X. Lin, J. D. Joannopoulos, M. Soljačić, and H. Chen, “Formation mechanism of guided resonances and bound states in the continuum in photonic crystal slabs,” *Sci. Rep.* **6**, 31908 (2016).
- [19] E. N. Bulgakov and A. F. Sadreev, “Robust bound state in the continuum in a nonlinear microcavity embedded in a photonic crystal waveguide,” *Opt. Lett.* **39**, 5212–5215 (2014).
- [20] S. I. Azzam, V. M. Shalaev, A. Boltasseva, and A. V. Kildishev, “Formation of bound states in the continuum in hybrid plasmonic-photonic systems,” *Phys. Rev. Lett.* **121**, 253901 (2018).
- [21] J. Jin, X. Yin, L. Ni, M. Soljačić, B. Zhen, and C. Peng, “Topologically enabled ultra-high-q guided resonances robust to out-of-plane scattering,” *arXiv preprint arXiv:1812.00892* (2018).
- [22] Weijin Chen, Yuntian Chen, and Wei Liu, “Singularities and Poincaré indexes of electromagnetic multipoles,” *arXiv preprint arXiv:1901.04159* (2019).
- [23] D. R. Abujetas, A. Barreda, F. Moreno, J. J. Saenz, A. Litman, and J. A. Geffrin, J.-M. and Sanchez-Gil, “Brewster quasi bound states in the continuum in all-dielectric metasurfaces from single magnetic-dipole resonance meta-atoms,” *arXiv preprint arXiv:1902.07148* (2019).
- [24] Y. V. Kartashov, C. Milián, V. V. Konotop, and L. Torner, “Bound states in the continuum in a two-dimensional PT-symmetric system,” *Opt. Lett.* **43**, 575–578 (2018).
- [25] S. Romano, G. Zito, S. Managò, G. Calafiore, E. Penzo, S. Cabrini, A. Chiara De Luca, and V. Mocella, “Surface-enhanced raman and fluorescence spectroscopy with an all-dielectric metasurface,” *J. Phys. Chem. C* **122**, 19738–19745 (2018).
- [26] E. Bulgakov and A. Sadreev, “Trapping of light with angular orbital momentum above the light cone,” *Advanced Electromagnetics* **6**, 1–10 (2017).
- [27] C. Wei Hsu, Bo Zhen, S.-L. Chua, S. G. Johnson, J. D. Joannopoulos, and M. Soljačić, “Bloch surface eigenstates within the radiation continuum,” *Light Sci. Appl.* **2**, e84 (2013).
- [28] B. Zhen, C. W. Hsu, L. Lu, A. D. Stone, and M. Soljačić, “Topological Nature of Optical Bound States in the Continuum,” *Phys. Rev. Lett.* **113**, 257401 (2014).
- [29] C. W. Hsu, Bo Zhen, J. Lee, S.-L. Chua, S. G. Johnson, J. D. Joannopoulos, and M. Soljačić, “Observation of trapped light within the radiation continuum,” *Nature* **499**, 188 (2013).
- [30] P. Yu, A. S. Kupriianov, V. Dmitriev, and V. R. Tuz, “All-dielectric metasurfaces with trapped modes: group-theoretical description,” *arXiv:1812.10817 [physics.optics]* (2018).
- [31] L. Ni, Zh. Wang, Ch. Peng, and Zh. Li, “Tunable optical bound states in the continuum beyond in-plane symmetry protection,” *Phys. Rev. B* **94**, 245148 (2016).
- [32] H. Friedrich and D. Wintgen, “Interfering resonances and bound states in the continuum,” *Phys. Rev. A* **32**, 3231–3242 (1985).
- [33] J. Jackson, *Classical electrodynamics* (Wiley, 1999).
- [34] P. Grahm, A. Shevchenko, and M. Kaivola, “Electromagnetic multipole theory for optical nanomaterials,” *New J. Phys.* **14**, 093033 (2012).
- [35] S. S. Kruk, R. Camacho-Morales, L. Xu, M. Rahmani, D. A. Smirnova, L. Wang, H. H. Tan, C. Jagadish, D. N. Neshev, and Y. S. Kivshar, “Nonlinear optical magnetism revealed by second-harmonic generation in nanoantennas,” *Nano Lett.* **17**, 3914–3918 (2017).
- [36] A. B. Evlyukhin, C. Reinhardt, A. Seidel, B. S. Luk’yanchuk, and B. N. Chichkov, “Optical response features of Si-nanoparticle arrays,” *Phys. Rev. B* **82**, 045404 (2010).
- [37] A. I. Kuznetsov, A. E. Miroshnichenko, M. L. Brongersma, Y. S. Kivshar, and B. Luk’yanchuk, “Optically resonant dielectric nanostructures,” *Science* **354**, aag2472 (2016).
- [38] M. Panmai, J. Xiang, Z. Sun, Y. Peng, H. Liu, H. Liu, Q. Dai, S. Tie, and S. Lan, “All-silicon-based nanoantennas for wavelength and polarization demultiplexing,” *Opt. Express* **26**, 12344–12362 (2018).
- [39] K. Baryshnikova, D. Filonov, C. Simovski, A. Evlyukhin, A. Kadochkin, E. Nenasheva, P. Ginzburg, and A. S. Shalin, “Giant magnetoelectric field separation via anapole-type states in high-index dielectric structures,” *Phys. Rev. B* **98**, 165419 (2018).
- [40] P. C. Wu, C. Y. Liao, V. Savinov, T. L. Chung, W. T. Chen, Y.-W. Huang, P. R. Wu, Y.-H. Chen, A.-Q. Liu, N. I. Zheludev, and D. P. Tsai, “Optical anapole metamaterial,” *ACS Nano* **12**, 1920–1927 (2018).
- [41] Wei Hsu, *Novel Trapping and Scattering of Light in Resonant Nanophotonic Structures*, Ph.D. thesis (2015).
- [42] A. V. Poshakinskiy and A. N. Poddubny, “Optomechanical kerker effect,” *Phys. Rev. X* **9**, 011008 (2019).
- [43] H. K. Shamkhi, K. V. Baryshnikova, A. Sayanskiy, P. Kapitanova, P. D. Terekhov, A. Karabchevsky, A. B. Evlyukhin, P. Belov, Y. Kivshar, and A. S. Shalin, “Transverse scattering with the generalised

- kerker effect in high-index nanoparticles,” [arXiv preprint arXiv:1808.10708](#) (2018).
- [44] W. Liu and Y. S. Kivshar, “Generalized kerker effects in nanophotonics and meta-optics (invited),” *Opt. Express* **26**, 13085–13105 (2018).
- [45] C. F. Bohren and D. R. Huffman, *Absorption and scattering of light by small particles*. (Wiley, 1983) pp. xiv, 530 p.
- [46] K.S. Frizyuk, “Second harmonic generation in dielectric nanoparticles with different symmetries,” [arXiv preprint arXiv:1812.02988](#) (2018).
- [47] J. A. Stratton, *Electromagnetic Theory* (2007) pp. 392–423.
- [48] H. M. Doeleman, F. Monticone, W. den Hollander, A. Alù, and A. F. Koenderink, “Experimental observation of a polarization vortex at an optical bound state in the continuum,” *Nature Photonics* **12**, 397 (2018).
- [49] W. Hergert and M. Dane, “Group theoretical investigations of photonic band structures,” *Phys. Status Solidi (a)* **197**, 620–634 (2003).
- [50] K. Ohtaka and Yu. Tanabe, “Photonic band using vector spherical waves. I. various properties of bloch electric fields and heavy photons,” *J. Phys. Soc. Jpn.* **65**, 2265–2275 (1996).
- [51] K. Ohtaka and Yu. Tanabe, “Photonic bands using vector spherical waves. III. group-theoretical treatment,” *J. Phys. Soc. Jpn.* **65**, 2670–2684 (1996).
- [52] K. Sakoda, “Optical properties of photonic crystals (Springer series in optical sciences, vol. 80),” (2001).
- [53] S. Hayami, M. Yatsushiro, Y. Yanagi, and H. Kusunose, “Classification of atomic-scale multipoles under crystallographic point groups and application to linear response tensors,” *Phys. Rev. B* **98**, 165110 (2018).
- [54] A. Gelessus, W. Thiel, and W. Weber, “Multipoles and symmetry,” *J. Chem. Educ.* **72**, 505 (1995).
- [55] V. M Agranovich and V. Ginzburg, *Crystal optics with spatial dispersion, and excitons*, Vol. 42 (Springer Science and Business Media, 2013).
- [56] E.L. Ivchenko and G. Pikus, *Crystal Symmetry. In: Superlattices and Other Heterostructures.*, Vol. 110 (Springer Series in Solid-State Sciences, Springer, Berlin, Heidelberg, 1995).
- [57] J.P. Goss, “Categorisation of point groups by symmetry operations,” http://newton.ex.ac.uk/research/qsystems/people/goss/symmetry/CC_All.html.
- [58] Z. Huayong and H. Yiping, “Addition theorem for the spherical vector wave functions and its application to the beam shape coefficients,” *J. Opt. Soc. Am. B* **25**, 255–260 (2008).
- [59] G. Aubert, “An alternative to Wigner d-matrices for rotating real spherical harmonics,” *AIP Advances* **3**, 062121 (2013).
- [60] Q. Yang, S. Kruk, Y. K. Srivastava, K. Koshelev, R. Singh, J. Han, Y. Kivshar, and I. Shadrivov, “Dielectric Membrane Mie-Resonant Metasurfaces,” in *Proceedings of CLEO* (2019).
- [61] J. D. Joannopoulos, S. G. Johnson, J. N. Winn, and R. D. Meade, *Photonic Crystals: Molding the Flow of Light (Second Edition)*, 2nd ed. (Princeton University Press, 2008).
- [62] C. T. Tai, *Dyadic Green’s Functions in Electromagnetic Theory, IEEE Antennas and Propagation Group Newsletter*, 2nd ed. (Piscataway, N.J. IEEE Press, 1994).
- [63] L.-W. Li, P.-S. Kooi, M.-S. Leong, and T.-S. Yee, “Electromagnetic dyadic green’s function in spherically multilayered media,” *IEEE Transactions on Microwave Theory and Techniques* **42**, 2302–2310 (1994).
- [64] R. Alaei, C. Rockstuhl, and I. Fernandez-Corbaton, “Exact multipolar decompositions with applications in nanophotonics,” *Adv. Opt. Mater* **7**, 1800783 (2019).
- [65] R. C. Wittmann, “Spherical wave operators and the translation formulas,” *IEEE Transactions on Antennas and Propagation* **36**, 1078–1087 (1988).
- [66] B. Stout, “Spherical harmonic lattice sums for gratings. In: Popov E, editor. Gratings: theory and numeric applications.” *Institut Fresnel, Universite d’Aix-Marseille* **6** (2012).

Appendix A: Basic definitions

Vector spherical harmonics are defined as [45]

$$\mathbf{M}_{-1mn} = \nabla \times (\mathbf{r}\psi_{-1mn}), \quad (\text{A1})$$

$$\mathbf{N}_{-1mn} = \frac{\nabla \times \mathbf{M}_{-1mn}}{k}, \quad (\text{A2})$$

where

$$\psi_{1mn} = \cos m\varphi P_n^m(\cos\theta)z_n(kr), \quad (\text{A3})$$

$$\psi_{-1mn} = \sin m\varphi P_n^m(\cos\theta)z_n(kr) \quad (\text{A4})$$

$z_n(kr)$ can be replaced by spherical bessel function of any kind, and $P_n^m(\cos\theta)$ are associated Legendre polynomials.

Vacuum dyadic Green's function expansion in terms of vector spherical harmonics [62, 63]:

$$\hat{\mathbf{G}}_0(\mathbf{r}, \mathbf{r}') = \frac{ik_1}{4\pi} \sum_{n=1}^{\infty} \sum_{p_r=\pm 1} \sum_{m=0}^n (2-\delta_0) \frac{2n+1}{n(n+1)} \frac{(n-m)!}{(n+m)!} \cdot \left([\mathbf{M}_{p_rmn}^{(3)}(k_1, \mathbf{r}) \otimes \mathbf{M}_{p_rmn}^{(1)}(k_1, \mathbf{r}')] + [\mathbf{N}_{p_rmn}^{(3)}(k_1, \mathbf{r}) \otimes \mathbf{N}_{p_rmn}^{(1)}(k_1, \mathbf{r}')] \right), \quad r > r' \quad (\text{A5})$$

where superscripts (1) and (3) appear, when we replace $z_n(\rho)$ by spherical Bessel functions, and the spherical Hankel functions of the first kind, respectively, $\delta_0 = 1$ when $m = 0$, and $\delta_0 = 0$ when $m \neq 0$.

Spherical vectors $\mathbf{Y}_{p_i p_r mn}$ denote two types of functions, $\mathbf{X}_{p_r mn}$ and $\mathbf{Z}_{p_r mn}$, defined as [64]

$$\mathbf{X}_{-p_r mn} \left(\frac{\mathbf{k}}{k} \right) = \nabla \times \left(\mathbf{k} Y_{p_r mn} \left(\frac{\mathbf{k}}{k} \right) \right) \quad (\text{A6})$$

$$\mathbf{Z}_{p_r mn} \left(\frac{\mathbf{k}}{k} \right) = i \frac{\mathbf{k}}{k} \times \mathbf{X}_{-p_r mn} \left(\frac{\mathbf{k}}{k} \right) \quad (\text{A7})$$

where

$$Y_{1mn} = \cos m\varphi P_n^m(\cos\theta) \quad (\text{A8})$$

$$Y_{-1mn} = \sin m\varphi P_n^m(\cos\theta) \quad (\text{A9})$$

p_i is $(-1)^{n+1}$ for \mathbf{X} , and $p_i = (-1)^n$ for \mathbf{Z} . Note that the transformation behavior is similar for \mathbf{W} and \mathbf{Y} , \mathbf{X} and \mathbf{M} , \mathbf{Z} and \mathbf{N} , ψ and Y , respectively.

Appendix B: Lattice sums of the spherical harmonics

We assume that multipolar content of the mode is already known, and coefficients in the formula (1) are given. With help of vacuum dyadic Green's function $\hat{\mathbf{G}}_0$, we express the field outside the array

$$\begin{aligned} \mathbf{E}(\mathbf{r}) &= \frac{k_1^2}{4\pi} \int d^3\mathbf{r}'' \Delta\varepsilon(\mathbf{r}'') \hat{\mathbf{G}}_0(\mathbf{r}, \mathbf{r}'') \mathbf{E}^{in}(\mathbf{r}'') = \\ &= \frac{k_1^2}{4\pi} (\varepsilon_2 - \varepsilon_1) \sum_j \int_V d^3\mathbf{r}' \hat{\mathbf{G}}_0(\mathbf{r}, \mathbf{r}_j + \mathbf{r}') \mathbf{E}^{in}(\mathbf{r}_j + \mathbf{r}') \end{aligned} \quad (\text{B1})$$

where $k_1 = \sqrt{\varepsilon_1} \frac{\omega}{c}$ is vacuum wavevector, V is the single nanoparticle's volume.

Green's function can be also expressed in terms of vector spherical harmonics (see Appendix A). Using the property $\hat{\mathbf{G}}_0(\mathbf{r}, \mathbf{r}_j + \mathbf{r}', \omega) = \hat{\mathbf{G}}_0(\mathbf{r} - \mathbf{r}_j, \mathbf{r}', \omega)$, and substituting (1) into (B1), we obtain

$$\mathbf{E}(\mathbf{r}) = E_0 \sum_j \frac{ik_1^3(\varepsilon_2 - \varepsilon_1)}{(4\pi)^2} \sum_{p_i, p_r, n, m} \sum_{p'_i, p'_r, n', m'} (2 - \delta_0) \frac{2n+1}{n(n+1)} \frac{(n-m)!}{(n+m)!} D_{p'_i p'_r n' m'} \mathbf{W}_{p_i p_r mn}^{(3)}(k_1, \mathbf{r} - \mathbf{r}_j) \cdot e^{i(\mathbf{k}_b \cdot \mathbf{r}_j)} \int_V d^3 \mathbf{r}' [\mathbf{W}_{p_i p_r mn}^{(1)}(k_1, \mathbf{r}') \cdot \mathbf{W}_{p'_i p'_r m' n'}^{(1)}(k_2, \mathbf{r}')] \quad (\text{B2})$$

here superscript (3) stands for the outgoing spherical Hankel wave. Now we dwell on the case when the array is composed of spherical nanoparticles. Exploiting the VSH orthogonality properties, the integral over sphere can be taken analytically [47]. It is proportional to Kroneker delta $\delta_{p_i p'_i} \delta_{p_r p'_r} \delta_{mm'} \delta_{nn'}$ which removes one summation. Combining all coefficients including the intergral into \tilde{D} we obtain that the field outside the array is expressed with the formula:

$$\mathbf{E}(\mathbf{r}) = E_0 \sum_{p_i, p_r, m, n} \tilde{D}_{p_i p_r mn} \mathbf{W}_{p_i p_r mn}^{(3)}(k_1, \mathbf{r} - \mathbf{r}_j) \cdot e^{i(\mathbf{k}_b \cdot \mathbf{r}_j)}. \quad (\text{B3})$$

Note, that coefficient $\tilde{D}_{p_i p_r mn}$ is non-zero only if the harmonic with such numbers is presented in the field expansion inside the sphere. If the fields created by each unit cell are already known, we can also start the considerations from this formula.

To obtain formula (2) we exploit the Weyl identity for VSH expansion through the plane waves in case when $z_n(kr)$ is replaced by spherical hankel functions[65, 66]:

$$\mathbf{M}_{p_r mn}^{(3)}(k, \mathbf{r}) = \frac{i^{-n}}{2\pi k} \iint_{-\infty}^{\infty} dk_{||} \frac{e^{i(k_x x + k_y y \pm k_z z)}}{k_z} \left[\mathbf{X}_{p_r mn} \left(\frac{\mathbf{k}}{k} \right) \right], \quad (\text{B4})$$

$$\mathbf{N}_{p_r mn}^{(3)}(k, \mathbf{r}) = \frac{i^{-n}}{2\pi k} \iint_{-\infty}^{\infty} dk_{||} \frac{e^{i(k_x x + k_y y \pm k_z z)}}{k_z} \left[\mathbf{Z}_{p_r mn} \left(\frac{\mathbf{k}}{k} \right) \right]. \quad (\text{B5})$$

Sign before k_z is depends on z - sign. Redefining the harmonics, we have

$$\mathbf{W}_{p_i p_r mn}^{(3)}(k, \mathbf{r}) = \frac{i^{-n}}{2\pi k} \iint_{-\infty}^{\infty} dk_{||} \frac{e^{i(k_x x + k_y y \pm k_z z)}}{k_z} \left[\mathbf{Y}_{p_i p_r mn} \left(\frac{\mathbf{k}}{k} \right) \right], \quad (\text{B6})$$

where $k_z = \sqrt{k^2 - k_x^2 - k_y^2}$. Substituting this expansion into (B3), we get

$$\mathbf{E}(\mathbf{r}) = E_0 \sum_{j, p_i, p_r, n, m} \tilde{D}_{p_i p_r mn} \cdot e^{i(\mathbf{k}_b \cdot \mathbf{r}_j)} \cdot \frac{i^{-n}}{2\pi k_1} \iint_{-\infty}^{\infty} dk_x dk_y \frac{e^{i(\mathbf{k}(\mathbf{r} - \mathbf{r}_j))}}{k_z} \left[\mathbf{Y}_{p_i p_r mn} \left(\frac{\mathbf{k}}{k} \right) \right]. \quad (\text{B7})$$

This expansion helps us to apply the summation formula

$$\sum_j e^{i\mathbf{k}\mathbf{x}_j} = V_b \sum_{\mathbf{K}} \delta(\mathbf{k} - \mathbf{K}) \quad (\text{B8})$$

where \mathbf{K} is reciprocal lattice vector and V_b is the volume of the Brillouin zone ($\frac{(2\pi)^2}{d^2}$ for square lattice), and substituting (B8) into (B7), we obtain (2).

Appendix C: Relation between the coefficients D and \tilde{D}

The coefficients D in (B2) and \tilde{D} (B3) are connected by the formula

$$\tilde{D}_{p_i p_r mn} = \frac{ik_1^3}{(4\pi)^2} (2 - \delta_0) \frac{2n+1}{n(n+1)} \frac{(n-m)!}{(n+m)!} D_{p_i p_r mn} \sum_{p'_i, p'_r, n', m'} \int_V d^3 \mathbf{r}' (\varepsilon_2 - \varepsilon_1) [\mathbf{W}_{p_i p_r mn}^{(1)}(k_1, \mathbf{r}') \cdot \mathbf{W}_{p'_i p'_r m' n'}^{(1)}(k_2, \mathbf{r}')] \quad (\text{C1})$$

This formula describes both array of nanoparticles, and any photonic crystal slab, but in case of the array of spheres, the integral can be easily taken analytically.

Remark Here we give the dyadic Green's function $\hat{\mathbf{G}}_0(\mathbf{r}, \mathbf{r}')$ only for the case when $r > r'$. In case of photonic crystal slab or non-spherical particles, we also need the part of Green's function when $r' < r$ [63] to obtain the near-field. This will alter the intermediate calculations, since we have to compute the lattice sum for VSHs with spherical bessel functions. Nevertheless, the answer will have the same form.

We apply the orthogonality properties of vector spherical harmonics [47] [p.418], and consider integrals of magnetic and electric harmonics separately. Implementing the angular integration, we reduce the integral to the integral of r-dependent Bessel functions products, which also can be computed analytically. For magnetic harmonics we have

$$\tilde{D}_{p_i p_r m n}^M = i D_{p_i p_r m n}^M a^2 \varepsilon_1 [k_1^2 j_{n-1}(k_1 a) j_n(k_2 a) - k_1 k_2 j_{n-1}(k_2 a) j_n(k_1 a)] \quad (\text{C2})$$

where a is nanoparticle radius, and for electric

$$\begin{aligned} \tilde{D}_{p_i p_r m n}^N = i D_{p_i p_r m n}^N a^2 \varepsilon_1 & \left(\frac{n+1}{2n+1} [k_1^2 j_{n-2}(k_1 a) j_{n-1}(k_2 a) - k_1 k_2 j_{n-2}(k_2 a) j_{n-1}(k_1 a)] + \right. \\ & \left. + \frac{n}{2n+1} [k_1^2 j_n(k_1 a) j_{n+1}(k_2 a) - k_1 k_2 j_n(k_2 a) j_{n+1}(k_1 a)] \right) \quad (\text{C3}) \end{aligned}$$

Note that this expression turns to zero at some frequencies, so we can have zero \tilde{D} when D is non-zero. This refers to the anapoles of the spherical nanoparticles. The frequency where the anapole appears is the same as for single isolated nanoparticle.

If we have other type of surface, for example, photonic crystal slab with holes, or array of the cylinders, the orthogonality property can't be applied and the integral $\int_V d^3 \mathbf{r}' \Delta \varepsilon [\mathbf{W}_{p_i p_r m n}^{(1)}(k_1, \mathbf{r}') \cdot \mathbf{W}_{p'_i p'_r m'_l n'}^{(1)}(k_2, \mathbf{r}')]$ will mix some harmonics. However, all the harmonics, which admix, are already presented in the expansion of the field inside the cell. This will just alter the coefficients before the outgoing multipoles, but not the multipolar content.
